Surface Properties of Alkoxysilane Layers Grafted in Supercritical Carbon Dioxide

Susan Sananes Israel, Diane Rébiscoul, Michaël Odorico, Valérie Flaud, Andre Ayral

Surface properties of alkoxysilane layers grafted in supercritical carbon dioxide

Susan Sananes Israel[†], Diane Rébiscoul[†]. Michael Odorico[†], Valérie Flaud[‡], André Ayral[¥],*

[†]ICSM, CEA, CNRS, ENSCM, Univ Montpellier, Marcoule, France, [‡]ICGM, UMR 5253, Montpellier, Cedex 5, France, and [¥]Institut Européen des Membranes, UMR CNRS 5635, CC047, Université de Montpellier, F-34095 Montpellier Cedex 5, France

KEYWORDS: Surface functionalization, alkoxysilane, silica, supercritical carbon dioxide,

ABSTRACT. Silicon oxide surface properties can be easily modified by grafting alkoxysilane molecules. Here, we studied the structure and the morphology of ultrathin layers prepared by the grafting of alkoxysilanes having different head groups (thiol, amine and iodo) in supercritical carbon dioxide (SC CO_2) on model plane silicon oxide surfaces. Several characterization techniques (X-ray reflectivity - XRR, water contact angle, X-ray photoelectron spectroscopy - XPS and atomic force microscopy - AFM) were used to determine the physicochemical properties of the layers prepared at different temperatures. Moreover, for the first time, AFM peak force measurements were used to delve deeper into the determination of the structure of these ultrathin alkoxysilane layers. The results show that the grafting temperature and the nature of the head group strongly affect the morphology and the structure of the grafted layers. Dense monolayers, polycondensed layers and dense bilayers are obtained with 3-(mercaptopropyl)trimethoxysilane

(MPTMS) at 60 °C, with [3-(aminoethylamino)propyl]trimethoxysilane (AEAPTMS) between 40°C and 120 °C, and with 3-(iodopropyl)triethoxysilane (IPTES) at 120 °C, respectively.

Introduction

Functionalized silica materials are widely used in microelectronic[1–4], decontamination[5–13], medical[14–16], catalysis[17–20] and biosensor[21–23] applications. Indeed, the surface of silica can be easily tuned, leading to materials with various properties, depending on the molecule grafted. For instance, the ion retention capacity on silicon oxide surfaces can be enhanced by the grafting of alkoxysilane molecules[1,2,9,24]. The surface morphology and the structure of the grafted layers are the main drivers of processes occurring in various applications of functionalized silica (such as extraction, sensing….). Conventional organic solvent such as toluene can be used for the silanization reaction[25,26]. Nevertheless these solvents present economic and environmental drawbacks and supercritical fluids have emerged as a greener alternative[27]. Different works focused on the functionalization of silicon oxide surfaces by alkoxysilanes in SC CO_2 and more particularly in porous silica and silica nanoparticles[1,2,36–41,28–35]. In this study, we focused on the grafting of different alkoxysilanes in SC CO_2 on model plane silicon oxide surfaces. This green solvent has already proved its efficiency for the functionalization of silicon oxide surfaces [42–44]. Above its critical point (T=31 ºC P=74 bars), carbon dioxide is in a supercritical state, with physicochemical properties between those of the liquid and the gas states, such as zero surface tension, high diffusivity and low density. Moreover, alkoxysilanes are soluble in SC CO_2. These properties minimize the polycondensation of alkoxysilanes favoring the molecule transport to the SC CO_2/SiO_2 interface where the grafting process occurs.

Usually, the grafting of alkoxysilanes is done by silanization, resulting from different phenomena[44]: (i) the dissolution of the alkoxysilane in SC CO_2 and the molecule transport to the

silicon oxide surface; (ii) the alkoxysilane hydrolysis by the interfacial water; (iii.1) the condensation and self-assembly of the hydrolyzed molecule with the surface silanols; and/or (iii.2) the self-condensation of the molecule and its physisorption at the silicon oxide surface. These different reactions (Figure S1 in the Supporting Information) are simultaneous and depend on the alkoxysilane used and on the experimental parameters[32,41].

In this work, three organic molecules were chosen and grafted in the SC CO_2 process: 3-(mercaptopropyl)trimethoxysilane (MPTMS), which is already known to form self-assembled monolayers (SAMs) on the silicon oxide surface[2]; [3-(aminoethylamino)propyl]trimethoxysilane (AEAPTMS); and for the first time, 3-(iodopropyl)triethoxysilane (IPTES). Table S1 summarizes some physicochemical properties of these three molecules. The grafting of alkoxysilanes in SC CO_2 has already been studied and some structures have been proposed for a grafting of a monolayer of MPTMS[29] at 100 bars. Thus, in this study, a pressure of 100 bars was used during the grafting process. Indeed, this pressure is sufficient to graft MPTMS on silica planar surface. This is not the case in porous media, which for the best parameters to form MPTMS monolayers in mesoporous materials were found at T = 80 ºC and P = 250 bars [35].

Generally, the structure and morphology of these alkoxysilane layers are difficult to characterize precisely because of the small thickness of the layers. In this study, we propose a new methodology coupling several surface characterization techniques to determine the structure and morphology of layers prepared in silicon oxide flat surfaces. First, the classical properties of the layers, such as density, thickness, roughness, chemical composition and hydrophilicity, were determined using X-ray reflectivity (XRR), atomic force microscopy (AFM), X-ray photoelectron spectroscopy (XPS) and contact angle measurements. Second, their spatial organization was explored through a pioneer study by AFM in peak force mode. This method is currently used to obtain information about the adhesion parameters of polymers and thin films of 2 to 10 nm thick[45–48]. Here, it was used to delve

deeper into the determination of the structure of ultrathin layers between 1 and 2 nm. Finally, we summarize the effects of the temperature and the functional group of the molecule on the layer morphology.

Experimental section

Material preparation

After the comparison of the contact angle obtained on the silicon surface pre-treated with a Caro solution and a 10 wt% nitric acid solution under reflux for 24 h (Table S3), the nitric acid preparation was selected. Thus, the surface of silicon wafers (<100> p-doped from MEMC Electronic Materials) was activated using a 10 wt% nitric acid solution under reflux for 24 h and rinsed with ultrapure water. The obtained hydrated silicon oxide layer was approximately 7 to 9 Å thick (determined from XRR measurements). MPTMS and AEAPTMS were provided by Sigma Aldrich. IPTES was obtained by the halogen exchange of (3-chloroproyl)triethoxysilane and NaI according to the procedure described in the literature[49].

The SC CO_2 grafting process was performed with a SEPAREX supercritical fluid extractor (See Figure S2). The activated silicon wafer was placed in the stainless-steel reactor. Then, the process described in Figure S3 was applied at 40°C, 60°C, 80°C, 100°C and 120°C for each molecule: SC CO_2 was flowed at 30 g/min, and a pressure of 100 bars was maintained. The reaction pressure has been set to 100 bars according to previous results on silicon oxide thin layers[2]. After 5 minutes, a solution containing 1 wt% of the organic molecule (MPTMS or IPTES) diluted in acetone was mixed with the SC CO_2 at 1.75 g/min and flowed in the reactor for 15 min. Due to the gelation of AEAPTMS in contact with SC CO_2, a 1 mL glass vial of AEAPTMS was placed directly in the reactor before the beginning of the process. Finally, samples were rinsed with SC CO_2 for 5

minutes. At the end of the process, samples were stored under vacuum. Samples were named X-Y, with X equal to MPT, AEA and IPT for MPTMS, AEAPTMS and IPTES, respectively, and Y equal to the grafting process temperature (in degree Celsius). The samples corresponding to the ungrafted silicon wafer with a hydrated silica layer were referenced Si-OH.

Sample characterization

X-ray reflectivity (XRR) analysis was used to determine the electron density profile of the samples. Measurements were carried out using a Bruker D8 diffractometer with CuKα1 (λ = 0.154056 nm) radiation. Standard θ–2θ scans for the data collections were taken from 2θ = 0º to 6º with an angular resolution of 0.01º. Reflectivity curves are usually presented as the evolution of the logarithm of intensity received by the detector as a function of the wave vector transfer $q = \frac{4\pi \sin\theta}{\lambda}$ with θ as the incident angle. Experimental curves were fitted using Firefx4c_6 software based on the Parratt algorithm in order to obtain electron density profiles and thus the thickness and the electron density of the prepared layer.

X-ray photoelectron spectrometry was performed using an ESCALAB 250 apparatus from ThermoElectron with a monochromatic Al Kα =1486.6 eV electron source. The takeoff angle for this spectrometer is 90º. Photoelectron spectra were calibrated to the C1s energy of the C-C bond at 284.8 eV. The background signal was obtained by the Shirley method[50]. The Si2p XPS spectra were decomposed with two contributions for the reference sample Si-OH and three contributions for the grafted samples[51]. It has been performed with the software Advantages from ThermoElectron, considering the silicon wafer Si-Si (99.0 eV), the SiO2 layer Si(-O)4 (102.7 eV) and the silicon from the grafted molecules Si(-O)3 (102.1 eV). The spectra were fitted with two Gauss-Lorentzian functions per contribution, corresponding to Si2p ½ ant Si2p 3/2 orbitals. These two peaks were fitted taking into account several conditions:

- The Full Width at Half Maximum is the same for the two Gauss-Lorentzian functions;
- The Area (A) of the Gauss-Lorentzian function Si2p3/2 is twice the area of the Gauss-Lorentzian function Si2p1/2: $A_{Si2p3/2}=2\ A_{Si2p1/2;}$
- For binding energy (BE) $BE_{Si2p3/2}= BE_{Si2p1/2}$ -0.6 eV.

Moreover, the FWHM and BE for the contributions Si-Si and $Si(-O)_4$ were fixed for all samples.

Water contact angle measurements were done using a Kruss Drop Shape Analyzer DSA100. A 10 µL drop was deposited on the sample, and the contact angle was measured using the Young-Laplace method. The measurements were repeated 3 times.

The roughness of the grafted silicon oxide surfaces was obtained by atomic force microscopy using an AFM Multimod8 with Nanoscope V from Brüker. The peak force measurements were performed with the same triangular SNL silicon tip from Brüker (spring constant of 350 pN/nm). All the measurements were performed in the same laboratory atmosphere (same relative humidity.) in order to avoid artefacts of the water meniscus [52]. Cantilever calibration was performed by the thermal tune method with a hard "naked" silicon substrate and the spring constant was set to 280 pN/nm. For each sample, force curves were measured on 30 points. The resulting force curves were divided on an approach curve and a retract curve related to the tip-surface attraction and tip-surface adhesion, respectively. We focus on two different data extracted from the retract curve: the adhesion length (L) and the adhesion force (F). The principle of the peak force measurements is explained in Figure S4. The profile of the force curve depends on the adhesion forces between the tip and the elaborated layer[53].

Results and Discussion

Figures 1 and 2 present the evolution of the contact angle, the electron density and the thickness of the grafted layer obtained from the fits of the X-ray-reflectivity curves and the AFM images, respectively. In the non-grafted sample, the presence of some organic contaminations can be characterized by XPS (Figure S7). The experimental and fitted X-ray reflectivity curves of the samples and the electron density profiles obtained from the fit are presented in Figure S5 and the parameters extracted from the grafted layer (thickness, electron density, roughness and contact angle) are present in the Table S2 of the supplementary data To determine the grafted molecules density in the layer, we have used the methodology presented in the experimental part. The results of the fit of the Si2p XPS spectra are reported in Table 1. The fitted curves are also available in Figure S6. The ratio between Si-Si and $Si(-O)_4$ $R = \frac{atom\%_{Si-Si}}{atom\%_{Si(-O)4}}$ remains around 0.2 for all the samples, indicating that the activated SiO_2 sublayer is the same for all the grafted layers. To compare the grafted alkoxysilane density on the different samples, the factor r ($Å^{-1}$) representing the density of grafted alkoxysilane in the layer was calculated as follows (1):

$$r = \frac{atom\%_{Si(-O)3}}{atom\%_{Si(-O)4}} \times \frac{1}{th} \quad (1)$$

where *th* is the thickness (Å) of the layer resulting from the fit of the reflectivity data.

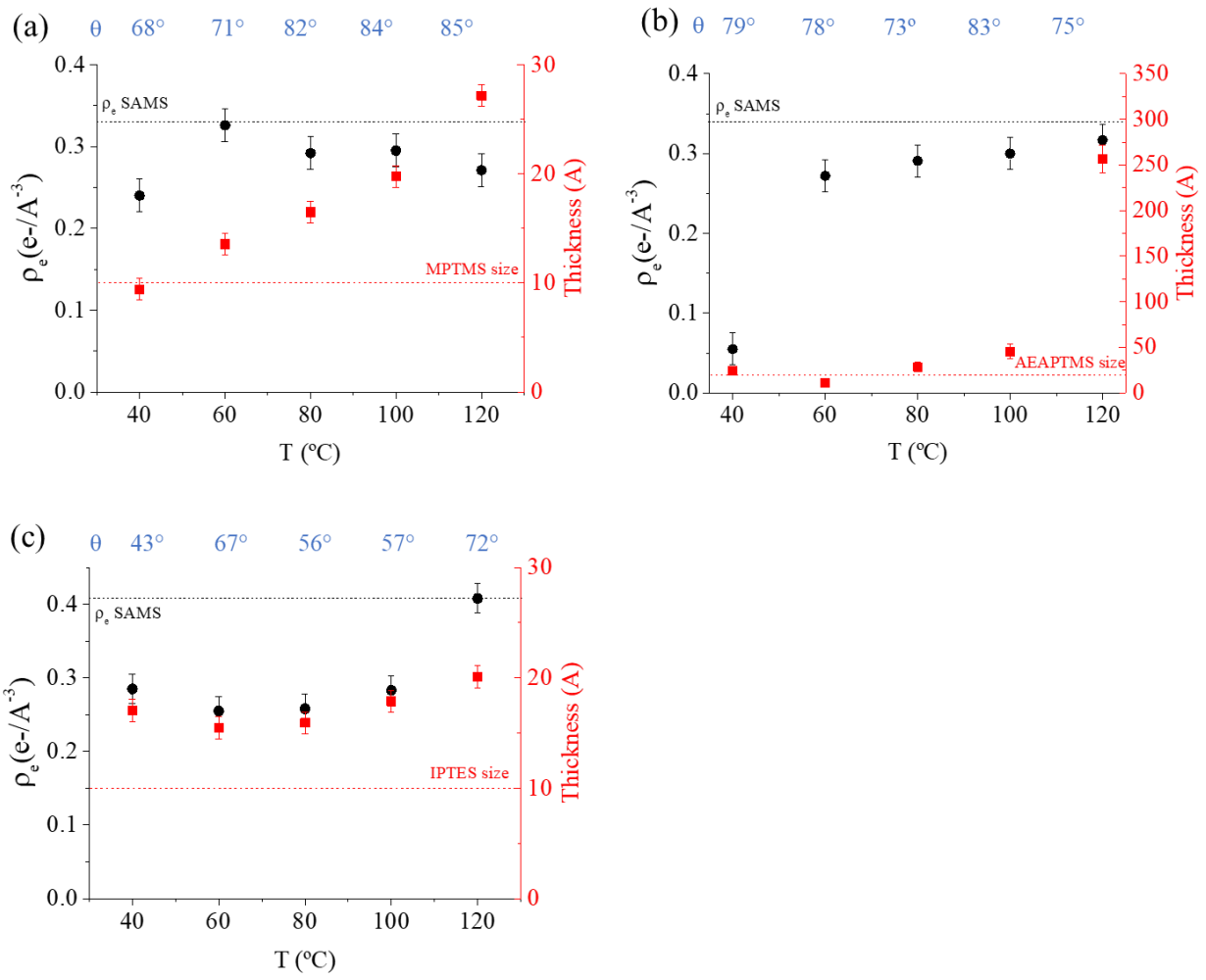

Figure 1. Evolutions of the electron density and the thickness of the grafted layers of (a) MPTMS, (b) AEAPTMS and (c) IPTES as a function of the process temperature. The contact angles θ are also given for each sample. The ρ_{SAMs} calculation is indicated in Table S1.

Table 1. Results of the decomposition of the Si2p peak for Si-OH, MPT-60, AEA-60, IPT-80 and IPT-120 samples.

Bond type	**Binding Energy**	**Si-OH**	**MPT-60**	**AEA-60**	**IPT-80**	**IPT-120**
	eV	%at	%at	%at	%at	%at
Si-Si	99.0	86.5	77.7	79.3	82.2	64.8
$Si(-O)_4$	102.7	13.5	15.2	16.0	13.1	19.4
$Si(-O)_3$	102.1		7.2	4.6	4.7	15.8
R		0.2	0.2	0.2	0.2	0.3
r ($Å^{-1}$)			0.034	0.026	0.022	0.041

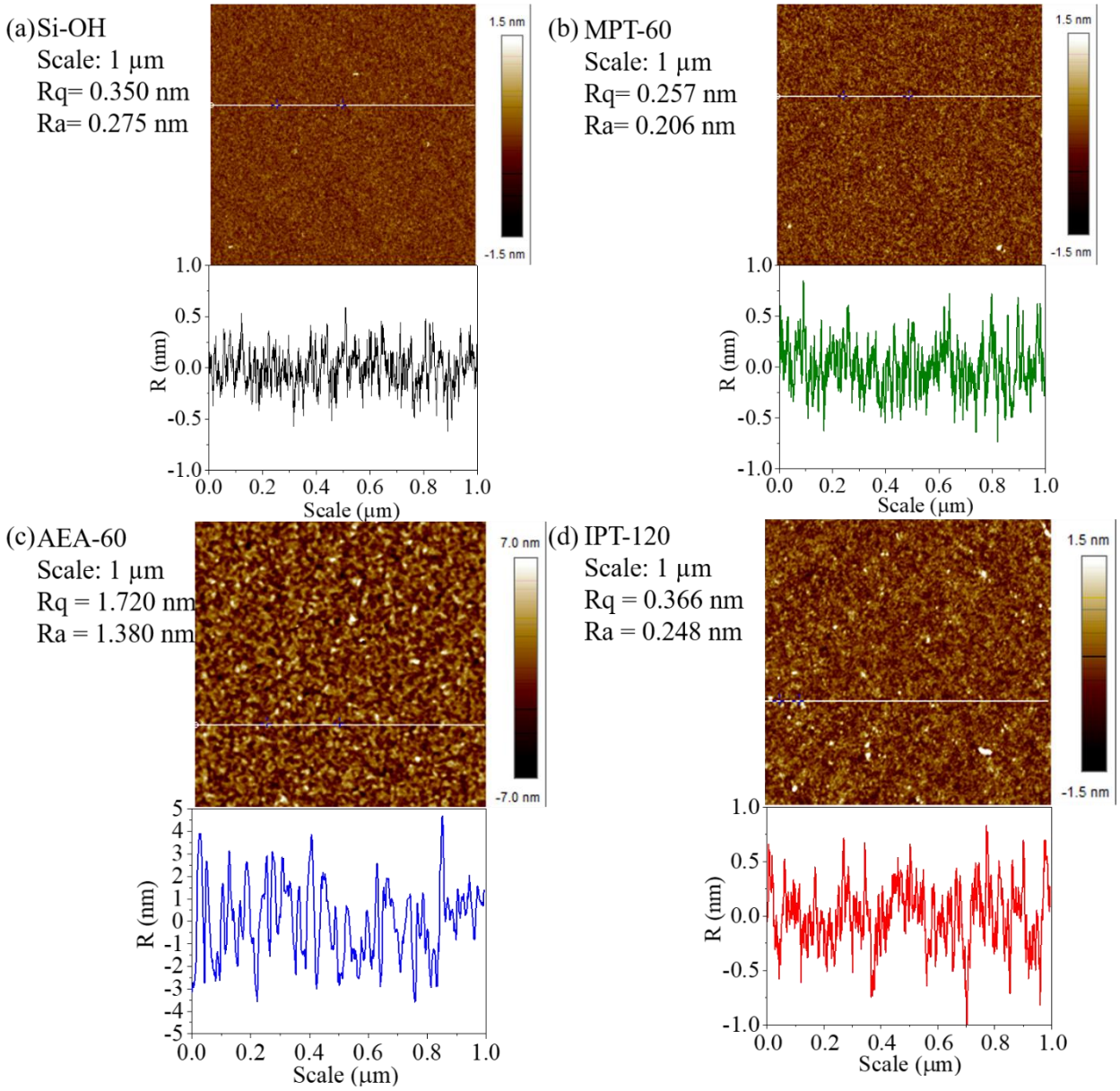

Figure 2. AFM images and topography profiles of Si-OH, MPT-60, AEA-60 and IPT-120 samples.

MPTMS grafting

The grafting of MPTMS leads to a linear increase in the layer thickness with the grafting temperature (Figure 1.a.). The electron density is lower than the theoretical value of liquid MPTMS (0.33 e-.Å^{-3}) except for MPT-60. At temperatures lower than 60°C, the layer is less dense than a grafted monolayer and close to the monolayer thickness. This may be due to a partial filling of the

monolayer. Above 60°C, polycondensed layers are obtained as they are thicker and less dense than the monolayer value. Additionally, the measured contact angles are higher than those for the MPTMS SAM (69-71º)[27]. These results enhance the possibility of a polycondensed layer formation. For grafting at 60°C, both the electron density and the thickness of the grafted layer are consistent with the density and the length of the grafted molecule (10 Å)[2]. This is also confirmed by the contact angle value approximately 70°[27] and the AFM images (Figures 2.a and 2.b) showing no surface modification after silanization. The roughness of the Si-OH sample (Ra=0.275 nm) is in agreement with values obtained in a previous work on silicon oxide surfaces (Ra=0.280 nm)[2]. Moreover, the structure of the MPT-60 is confirmed by XPS with a peak of weak intensity from the S2s binding energy, confirming the presence of the MPTMS molecule (Figure 3). Its low intensity can be explained by the monolayer structure, since sulfur atoms account for 0.01 % to 0.02 % of the probed zone (from 5 to 10 nm). In addition, as previous results suggest that a monolayer is obtained, the calculated ratio of r equal to 0.034 $Å^{-1}$ (Table 1) will be used as a reference for a monolayer.

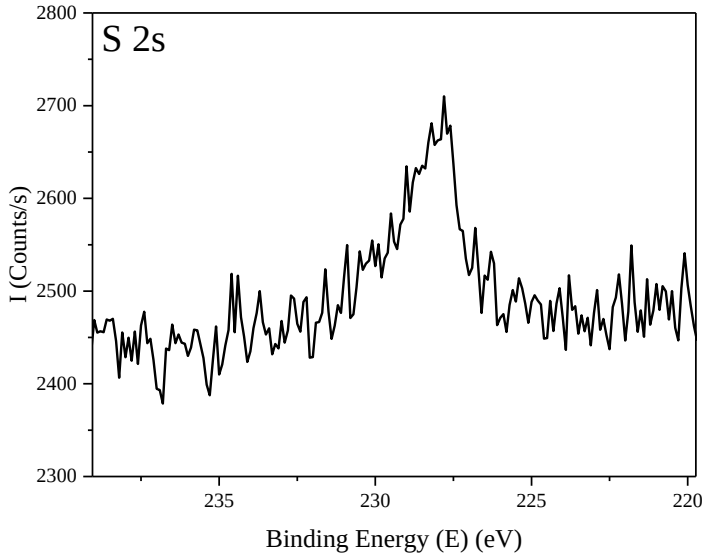

Figure 3. S2s XPS spectra of MPT-60.

The peak force measurements performed by AFM also suggest the presence of a monolayer on the MPT-60 sample. Indeed, the 30 force curves displayed in Figure 4.a are very similar. There is a strong vertical jump on the retract curve at L=12.3 nm and an adhesion force of F=-3.3 nN. When the tip retracts to the surface, the layer is submitted to tension, resulting from the surface-tip adhesion.

With increased linkage in the layer, a greater force is required to break the bonds, and the adhesion length is short, (Figure 4.b.). In MPT-60, the tip-surface adhesion is homogeneous across the entire surface, as the force curves are very similar. All of this experimental evidence suggests that MPTMS forms a monolayer at 60°C. These results are in agreement with a previous work on silicon oxide surfaces[2]

(a)

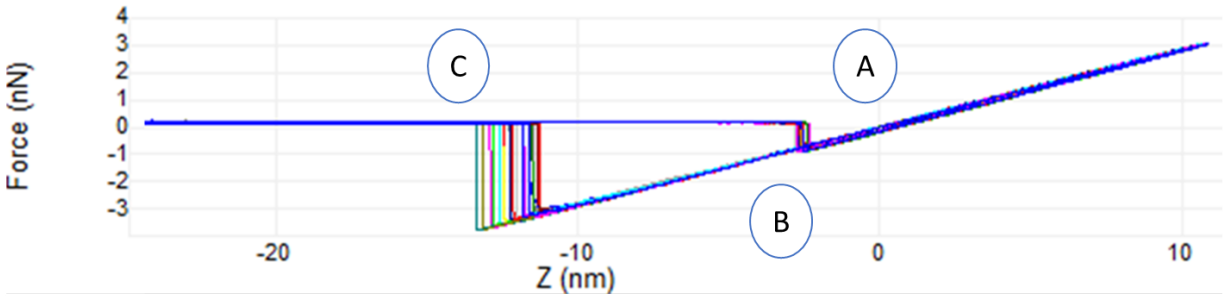

(b)

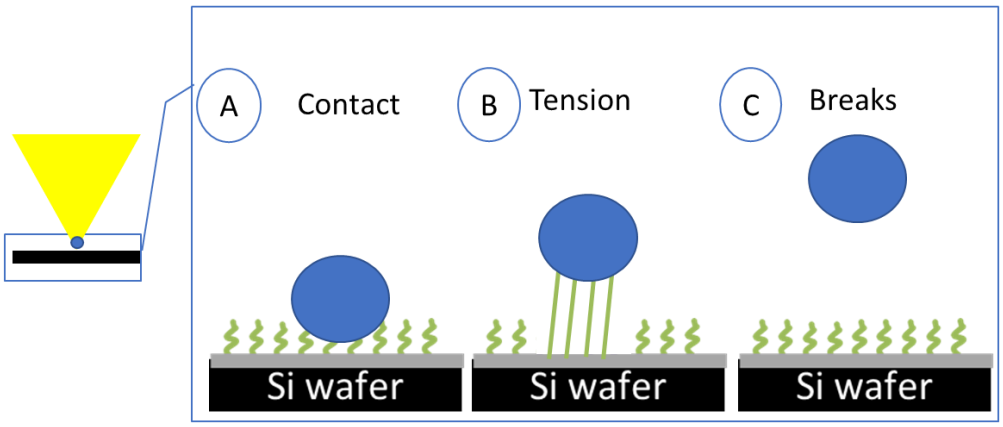

Figure 4. AFM peak force curves of MPT-60 (a) and schematic representation of possible phenomena occurring during the peak force measurements of a MPTMS monolayer (b).

AEAPTMS grafting

For process temperatures ranging from 60°C to 120°C, the grafted layer thickness increases, but its polycondensed structure remains the same. Indeed, all the AEAPTMS grafted layers have similar electron densities below the theoretical electron density (0.32 e-. $Å^{-3}$) and a thickness higher than the length of the AEAPTMS molecule (20 Å) above 60ºC (Figure 1.b). Moreover, the roughness obtained by the fit of the experimental X-ray reflectivity curves increases with the grafting process temperature. The contact angle remains between 73° and 83°. The values obtained

are similar to those from a previous work[2] but are not consistent with a monolayer containing surface amino groups, as the contact angle expected for an amine is near 36°[27]. The results suggest that AEAPTMS grafted layers are rather polycondensed.

These results are confirmed by the AFM images of the AEA-60 sample (Figure 2.c), showing a higher roughness than the MPT-60 sample. Moreover, AEA-60 has a lower grafting ratio r than MPT-60 (0.026 $Å^{-1}$ vs 0.034 $Å^{-1}$) (Table 1). This result confirms that the density of alkoxysilanes in the layer is lower than in a monolayer. Furthermore, the N1s peak was also decomposed into three contributions[2] (Figure 5.a.): the amine from the head group -NH_2 (399.3 eV), the amine inside the alkyl chain -NH- (400.5 eV) and the amine hydrogen-bonded to a surface silanol -NH_2…HO- (401.6 eV). This last contribution is assigned to the hydrogen bond of the amine with surface silanols or with other hydroxylated molecules. Its presence indicates that AEAPTMS is not self-aligned at the silicon oxide surface and that some of the amine head groups are probably oriented towards the silicon oxide layer, exposing hydrolyzed silanol groups on the surface[54]. This fact probably accelerates the polycondensation of the layer.

Moreover, the AFM peak force analysis performed on the AEA-60 sample (Figure 6.a) shows that the adhesion force is weaker (F= -1.84 nN) and the adhesion length is higher (L=17.4 nm) than those of the MPT-60 sample. This means that the grafted AEAPTMS layer is less linked to the surface than the MPTMS in a monolayer. As the prepared layer is polycondensed, the inhomogeneous tip-surface adhesion leads to random bond breaking, resulting from a larger retract curve (Figure 6.b).

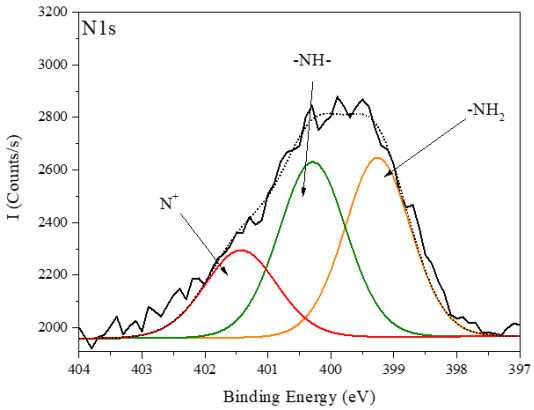

Figure 5. N1s XPS spectra of AEA-60 sample.

(a)

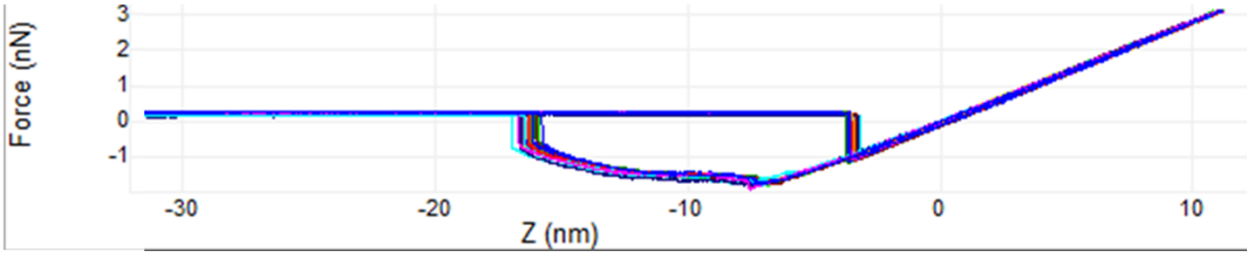

(b)

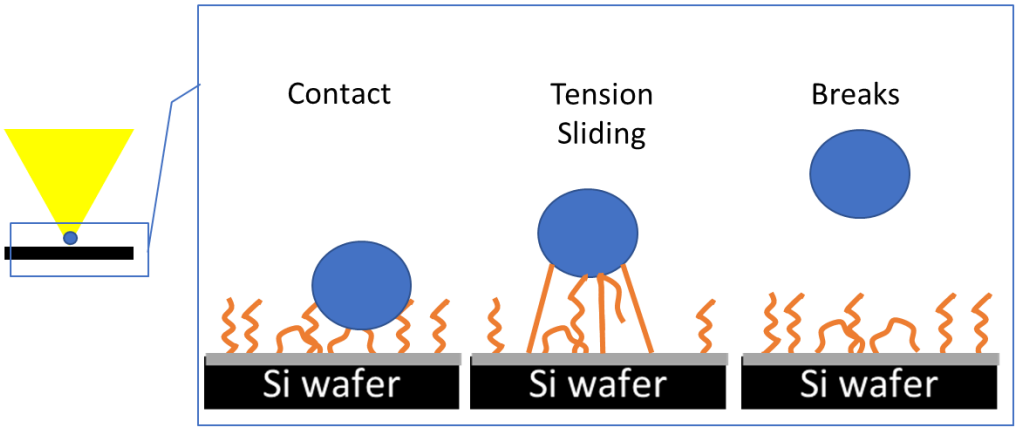

Figure 6. AFM peak force curves of AEA-60 (a) and schematic representation of possible phenomena occurring during the peak force measurements of a polycondensed layer (b).

IPTES grafting

Regardless of the temperature, the IPTES grafted layers present thicknesses close to twice the molecule length (Table S1), and the densities are lower than that of liquid IPTES (0.42 e-.$Å^{-3}$), except for IPT-120 (Figure 1. c). Moreover, the roughness obtained by the fit of the experimental X-ray reflectivity curves is constant whatever the grafting process temperature and close to the one of the monolayer of MPTMS. The AFM images show that the IPT-120 sample is not modified after the grafting process, with a roughness similar to that of the non-grafted sample (Figure 2). For the IPT-120 sample, the XRR and AFM results could suggest the presence of a grafted bilayer, which has the density of liquid IPTES with the presence of scattered nanoagglomerates at the surface. Moreover, the I3d XPS spectra of IPT-80 and IPT-120 samples (Figure 7) show the presence of the iodine peak of the IPTES molecule.

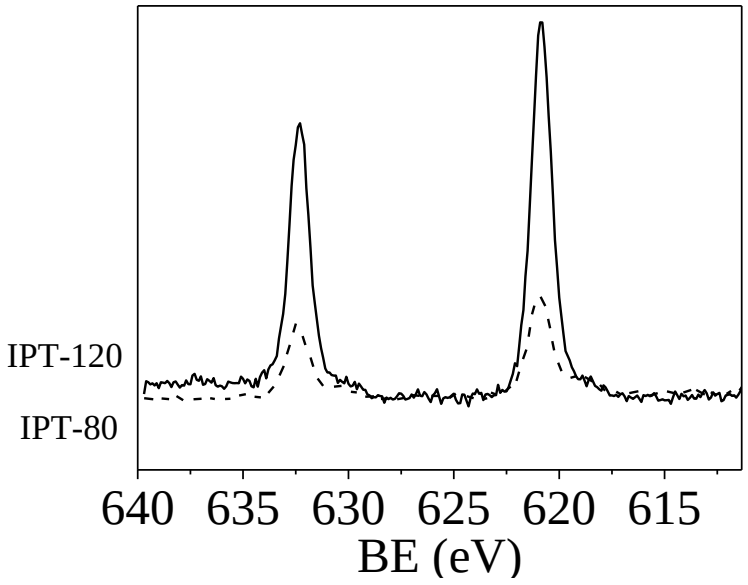

Figure 7. I3d XPS spectra (a) (b) of IPT-80 and IPT-120 samples.

Regarding these results, several bilayer structures can be proposed (Figure 8.) Indeed, the iodine present in the IPTES molecule can interact as a Lewis base with hydrogen atoms from the surface silanols[54] and/or from another hydrolyzed IPTES molecule (Figure 8.a) and/or with hydrogen atoms from the alkyl chain. Otherwise, it is possible to have an interpenetration of two monolayers in a comb-type structure (Figure 8.b).

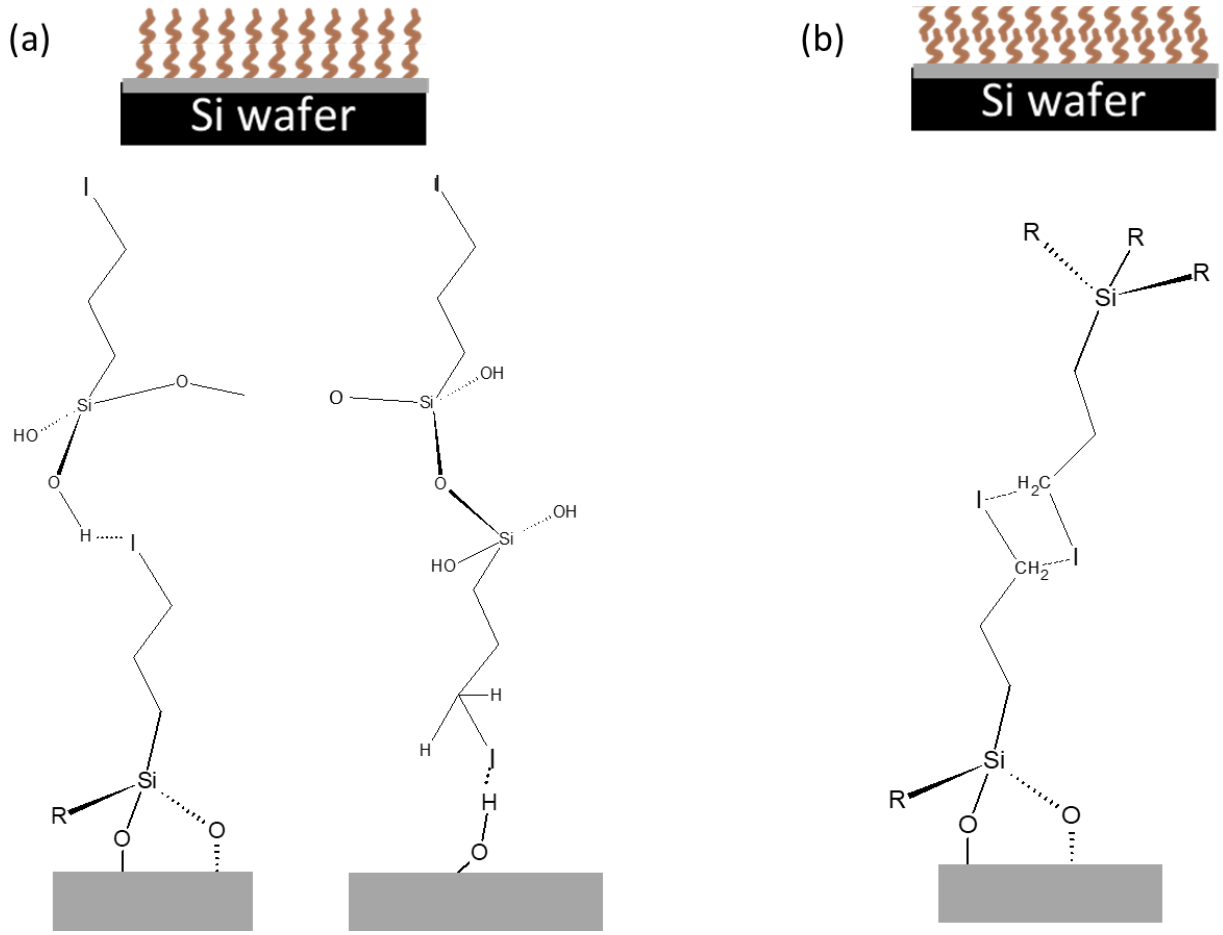

Figure 8. Possible conformations for the IPTES molecules in IPT-120 sample. R = OH or OCH_3 in the case of a bilayer.

.

However, r obtained from XPS is lower for IPT-80 (0.022 $Å^{-1}$) than for IPT-120 (0.041 $Å^{-1}$) (Table 1), attesting to the lower density of IPTES in the IPT-80 than in the IPT-120 sample. For IPT-120, r is higher than the r of the monolayer of the MPT-60 sample. According to this result, it is possible that a bilayer presenting an interpenetration of two monolayers was obtained. In addition, contact angles ranged from 58° to 66º for the different prepared layers except for IPT-120 (75°). This increase in contact angle for IPT-120 may suggest the formation of a dense and interpenetrated bilayer. We have also to precise that the few scattered nanoaglomerates at the surface could also increase the contact angle.

When comparing the different AFM peak force curves of the IPT-80 and IPT-120 samples, only small differences in the adhesion length and adhesion force values are observed (Figure 9): Z=13.8 nm; F=-1.83 nN for IPT-80 vs. Z=12.1 nm; F=-2.36 nN for IPT-120 sample. The increase in the adhesion force with temperature may indicate that the layer is more bonded to the silicon oxide surface for IPT-120. Nevertheless, the adhesion force in MPT-60 sample is higher than that for IPT-120. This can indicate that the molecule is not as linked to the surface as in MPT-60.

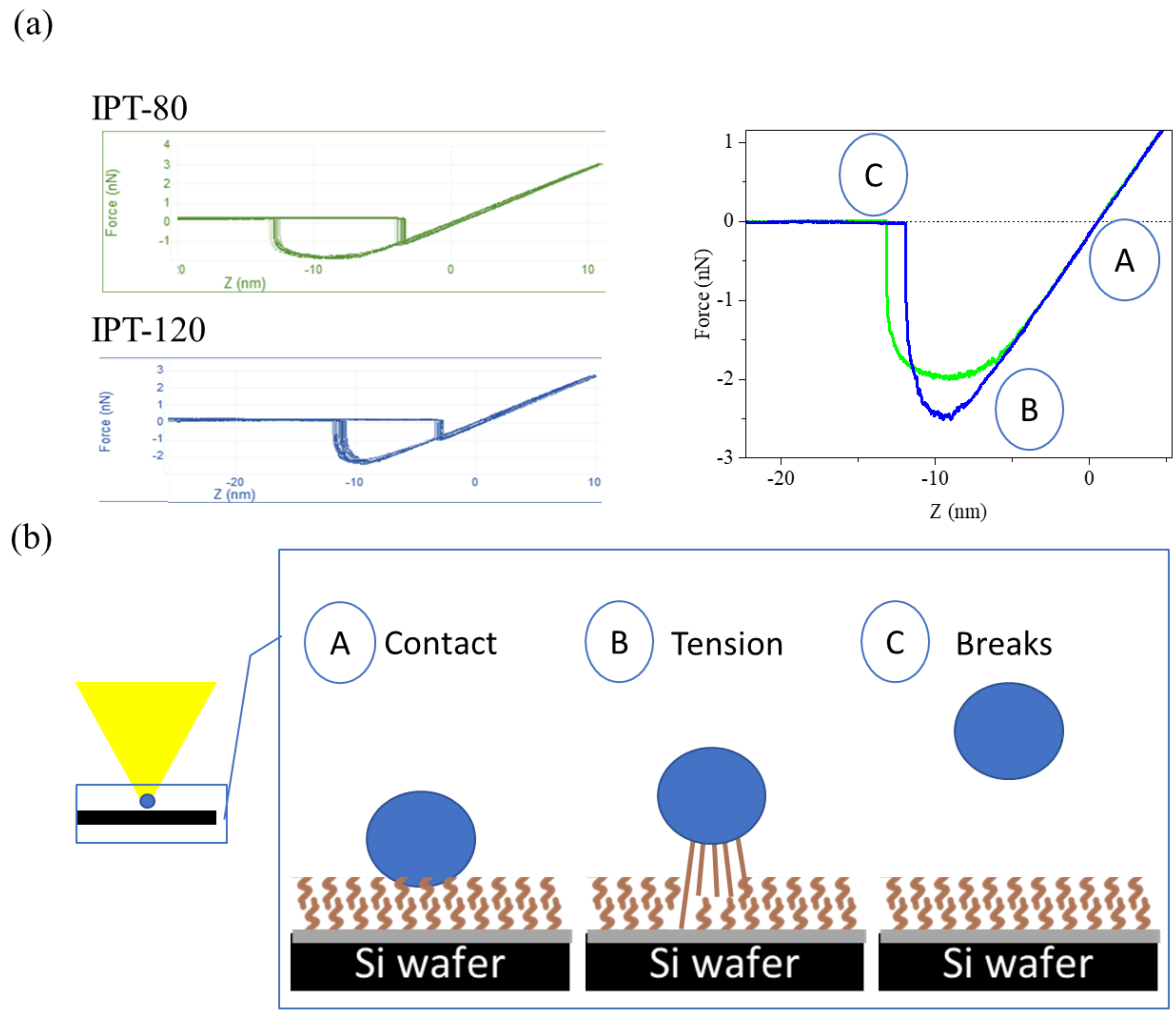

Figure 9. AFM peak force curves of IPT-80 (green) and IPT-120 (blue) samples (a). One retract curve of each sample is plotted on the right graph. Schematic representation of possible phenomena occurring during the peak force measurement of the IPT-120 (b) sample.

Summary on the effects of temperature and functional group on the morphology of the grafted layer

Here, we discuss the structure of the grafted layer, which depends on the functional groups and the temperature. Figure 10 illustrates the different layer morphologies obtained as a function of

temperature. The MPTMS monolayer is probably formed through the classical silanization reaction [2,44,55]. First, alkoxysilanes are hydrolyzed by the water on the extreme silicon oxide surface. Then, the molecule bonds to surface silanols. Finally, the self-assembly between the molecules gives a homogeneous monolayer. When the temperature is above 60ºC, molecules self-react before they reach the O-H surface groups, leading to disorganized and low-density layers.

In the case of AEAPTMS, in addition to the self-condensation of the grafted molecules with an increase in temperature leading to thicker layers, there is also an effect of the attraction between the amine and the silicon oxide surface. This attraction of the head group to the silicon oxide surface favors the formation of a disorganized layer regardless of the temperature. Nevertheless, the increase of the layer thickness indicates that the self-polymerization of the alkoxysilane is promoted at high temperatures.

With IPTES, the CO_2 SC grafting process probably leads to a bilayer presenting an interpenetration of two monolayers. The density of this bilayer increases with the temperature until its complete filling at 120°C.

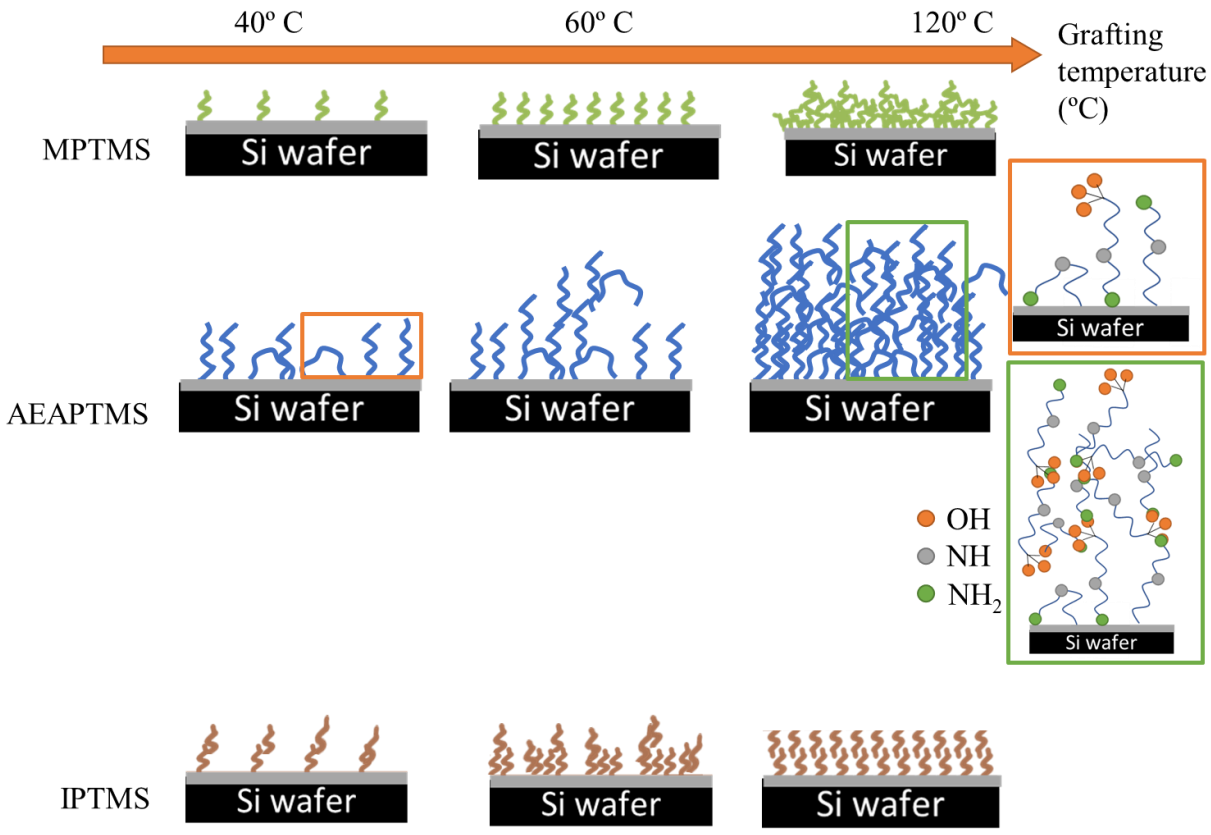

Figure 10. Schematic representations of the morphology for the prepared layers of MPTMS (top), AEAPTMS (middle) and IPTES (bottom) as a function of the grafting temperature.

Summary and conclusions

For the first time, the morphology and the structure of the alkoxysilane grafted layer on silica plane surface were finely characterized by implementing different complementary techniques and the AFM peak force measurements. The SC CO_2 grafting of IPTES has also been reported as a novelty. The experimental data show that the grafting temperature and the nature of the head group are the main parameters affecting their morphology and structure. While dense monolayers are grafted with MPTMS at 60ºC, polycondensed layers with AEAPTMS and dense bilayers with IPTES at 120ºC are obtained. Some ab initio calculations are ongoing to determine the possible conformations in a case of a bilayer. While the alkoxysilane grafting in SC CO_2 was already studied

in porous materials [1,2,36–41,28–35], the impact of the confinement was not determined. In order to investigate this confinement effect, nanochannels[56] made of two silicon oxide plane surfaces spaced of 3 and 5 nm will be grafted with the same molecules and will be then characterized using X-ray reflectivity. The obtained results should help us to evidence a possible confinement effect (pore size and diffusion path) on the grafting efficiency and also on the morphology of the grafted layer. The influence of the pressure on the morphology of these layers can also be of great interest for evaluating the impact of changes in the SC CO_2 properties such as diffusion coefficient and density.

Acknowledgments. This work was supported by Université de Montpellier and Commissariat à l'Energie Atomique. We are grateful to Bruno Corso for XRR maintenance.

Supporting Information. Physicochemical properties of the grafted alkoxysilanes, explanations on the experimental set-up, XRR and XPS curves and the results of the fit can be found in the supporting information

(1) Perrut, V.; Morel, T.; Cubitt, R.; Horowitz, J.; Rébiscoul, D.; Jayet, C.; Haumesser, P. H. Alkoxysilane Layers Compatible with Copper Deposition for Advanced Semiconductor Device Applications. *Langmuir* **2010**, *26* (11), 8981–8987.

(2) Rébiscoul, D.; Perrut, V.; Renault, O.; Rieutord, F.; Olivier, S.; Haumesser, P. H. Alkoxysilane Layers Deposited by SC CO 2 Process on Silicon Oxide for Microelectronics Applications. *J. Supercrit. Fluids* **2009**, *51* (2), 287–294.

(3) Weibel, G. L.; Ober, C. K. An Overview of Supercritical CO2applications in Microelectronics Processing. *Microelectronic Engineering*. 2002, pp 145–152.

(4) Ciaramella, F.; Jousseaume, V.; Maitrejean, S.; Verdier, M.; Remiat, B. Crosslinking Impact of Mesoporous MSQ Films Used in Microelectronic Interconnections on Mechanical Properties. **2006**, *495*, 124–129.

(5) Zub, Y. L.; Viltuz, B.; Lobnik, A. Removal of Pb (II) Ions from Aqueous Systems Using Thiol- Functionalized Cobalt-Ferrite Magnetic Nanoparticles. **2013**, 365–373.

(6) Benhamou, A.; Baudu, M.; Derriche, Z.; Basly, J. P. Aqueous Heavy Metals Removal on Amine-Functionalized Si-MCM-41 and Si-MCM-48. *J. Hazard. Mater.* **2009**, *171* (1–3), 1001–1008.

(7) Xue, X.; Li, F. Removal of Cu(II) from Aqueous Solution by Adsorption onto Functionalized SBA-16 Mesoporous Silica. *Microporous Mesoporous Mater.* **2008**, *116* (1–3), 116–122.

(8) Gascón, V.; Aguado, J.; Arsuaga, J. M.; Arencibia, A.; Lindo, M.; Gascón, V. Aqueous Heavy Metals Removal by Adsorption on Amine-Functionalized Mesoporous Silica. *J.*

Hazard. Mater. **2009**, *163* (1), 213–221.

(9) Bois, L.; Bonhommé, A.; Ribes, A.; Pais, B.; Raffin, G.; Tessier, F. Functionalized Silica for Heavy Metal Ions Adsorption. *Colloids Surfaces A Physicochem. Eng. Asp.* **2003**, *221* (1–3), 221–230.

(10) Lee, B.; Kim, Y.; Lee, H.; Yi, J. Synthesis of Functionalized Porous Silicas via Templating Method as Heavy Metal Ion Adsorbents: The Introduction of Surface Hydrophilicity onto the Surface of Adsorbents. *Microporous Mesoporous Mater.* **2001**, *50* (1), 77–90.

(11) Mureseanu, M.; Reiss, A.; Stefanescu, I.; David, E.; Parvulescu, V.; Renard, G.; Hulea, V. Modified SBA-15 Mesoporous Silica for Heavy Metal Ions Remediation. *Chemosphere* **2008**, *73* (9), 1499–1504.

(12) Mercier, L.; Pinnavaia, T. J. Heavy Metal Ion Adsorbents Formed by the Grafting of a Thiol Functionality to Mesoporous Silica Molecular Sieves: Factors Affecting Hg(II) Uptake. *Environ. Sci. Technol.* **1998**, *32* (18), 2749–2754.

(13) Makowski, P.; Deschanels, X.; Grandjean, A.; Meyer, D.; Toquer, G.; Goettmann, F. Mesoporous Materials in the Field of Nuclear Industry: Applications and Perspectives. *New J. Chem.* **2012**, *36* (3), 531.

(14) Ichiyanagi, Y.; Moritake, S.; Taira, S.; Setou, M. Functional Magnetic Nanoparticles for Medical Application. *J. Magn. Magn. Mater.* **2007**, *310* (2 SUPPL. PART 3), 2877–2879.

(15) Sanchez, C.; Shea, K. J.; Kitagawa, S.; Vallet-Regı, M.; Colilla, M.; Gonzaíez, B. Medical Applications of Organic–inorganic Hybrid Materials within the Field of Silica-Based Bioceramicsw. *Chem. Soc. Rev* **2011**, *40*, 596–607.

(16) Vallet-Regí, M.; Ruiz-González, L.; Izquierdo-Barba, I.; González-Calbet, J. M. Revisiting Silica Based Ordered Mesoporous Materials: Medical Applications.

(17) Yokoi, T.; Kubota, Y.; Tatsumi, T. Amino-Functionalized Mesoporous Silica as Base Catalyst and Adsorbent. *Appl. Catal. A Gen.* **2012**, *421–422*, 14–37.

(18) Conley, M. P.; Cope, C.; Thieuleux, C. Mesostructured Hybrid Organic − Silica Materials: Ideal Supports for Well-De Fi Ned Heterogeneous Organometallic Catalysts. **2014**.

(19) Shin, K. S.; Cho, Y. K.; Choi, J. Y.; Kim, K. Facile Synthesis of Silver-Deposited Silanized Magnetite Nanoparticles and Their Application for Catalytic Reduction of Nitrophenols. *Appl. Catal. A Gen.* **2012**, *413–414*, 170–175.

(20) Yokoi, T.; Kubota, Y.; Tatsumi, T. Applied Catalysis A : General Amino-Functionalized Mesoporous Silica as Base Catalyst and Adsorbent. *"Applied Catal. A, Gen.* **2012**, *421–422*, 14–37.

(21) Karimi, M.; Badiei, A.; Mohammadi Ziarani, G. A Single Hybrid Optical Sensor Based on Nanoporous Silica Type SBA-15 for Detection of Pb2+ and I- in Aqueous Media. *RSC Adv.* **2015**, *5* (46), 36530–36539.

(22) Slowing, I. I.; Trewyn, B. G.; Giri, S.; Lin, V. S. Y. Mesoporous Silica Nanoparticles for Drug Delivery and Biosensing Applications. *Adv. Funct. Mater.* **2007**, *17* (8), 1225–1236.

(23) Sarkar, K.; Dhara, K.; Nandi, M.; Roy, P.; Bhaumik, A.; Banerjee, P. Selective Zinc(II)-Ion Fluorescence Sensing by a Functionalized Mesoporous Material Covalently Grafted with a Fluorescent Chromophore and Consequent Biological Applications. *Adv. Funct. Mater.* **2009**, *19* (2), 223–234.

(24) Ruckenstein, E.; Li, Z. F. Surface Modification and Functionalization through the Self-Assembled Monolayer and Graft Polymerization. *Adv. Colloid Interface Sci.* **2005**, *113*, 43–63.

(25) Arkles, B. Tailoring Surfaces with Silanes. *Chemtech* **1977**, *7* (12), 766–778.

(26) Brzoska, J. B.; Azouz, I. Ben; Rondelez, F. Silanization of Solid Substrates: A Step toward Reproducibility. *Langmuir* **1994**, *10*, 4367–4373.

(27) Aswal, D. K.; Lenfant, S.; Guerin, D.; Yakhmi, J. V; Vuillaume, D. Self Assembled Monolayers on Silicon for Molecular Electronics. *Anal. Chim. Acta* **2006**, *568*, 84–108.

(28) Zemanian, T. S.; Fryxell, G. E.; Liu, J.; Mattigod, S.; Franz, J. A.; Nie, Z. Deposition of Self-Assembled Monolayers in Mesoporous Silica from Supercritical Fluids. *Langmuir* **2001**, *17* (26), 8172–8177.

(29) Tenorio, M. J.; Morère, J.; Carnerero, C.; Torralvo, M. J.; Pando, C.; Cabañas, A. Thiol Group Functionalization of Mesoporous SiO2 SBA-15 Using Supercritical CO2. *Microporous Mesoporous Mater.* **2018**, *256*, 147–154.

(30) Sánchez-Vicente, Y.; Stevens, L. A.; Pando, C.; Torralvo, M. J.; Snape, C. E.; Drage, T. C.; Cabañas, A. A New Sustainable Route in Supercritical CO2 to Functionalize Silica SBA-15 with 3-Aminopropyltrimethoxysilane as Material for Carbon Capture. *Chem. Eng. J.* **2015**, *264*, 886–898.

(31) López-Aranguren, P.; Fraile, J.; Vega, L. F.; Domingo, C. Regenerable Solid CO2 Sorbents Prepared by Supercritical Grafting of Aminoalkoxysilane into Low-Cost Mesoporous Silica. *J. Supercrit. Fluids* **2014**, *85*, 68–80.

(32) López-Aranguren, P.; Saurina, J.; Vega, L. F.; Domingo, C.; Lopez-Aranguren, P.; Saurina, J.; Vega, L. F.; Domingo, C.; López-Aranguren, P.; Saurina, J.; et al. Sorption of Tryalkoxysilane in Low-Cost Porous Silicates Using a Supercritical CO2 Method. *Microporous Mesoporous Mater.* **2012**, *148* (1), 15–24.

(33) Sun, D.; Liu, Z.; He, J.; Han, B.; Zhang, J.; Huang, Y. Surface Sol-Gel Modification of Mesoporous Silica Molecular Sieve SBA-15 with TiO2 in Supercritical CO2. *Microporous Mesoporous Mater.* **2005**, *80* (1–3), 165–171.

(34) Builes, S.; López-Aranguren, P.; Fraile, J.; Vega, L. F.; Domingo, C. Alkylsilane-Functionalized Microporous and Mesoporous Materials: Molecular Simulation and Experimental Analysis of Gas Adsorption. *J. Phys. Chem. C* **2012**, *116* (18), 10150–10161.

(35) Ashu-Arrah, B. A.; Glennon, J. D.; Albert, K. Synthesis and Characterisation of Bonded Mercaptopropyl Silica Intermediate Stationary Phases Prepared Using Multifunctional Alkoxysilanes in Supercritical Carbon Dioxide as a Reaction Solvent. *J. Chromatogr. A* **2012**, *1222*, 38–45.

(36) Stojanovic, D.; Orlovic, A.; Glisic, S. B.; Markovic, S.; Radmilovic, V.; Uskokovic, P. S.; Aleksic, R. Preparation of MEMO Silane-Coated SiO2 Nanoparticles under High Pressure of Carbon Dioxide and Ethanol. *J. Supercrit. Fluids* **2010**, *52* (3), 276–284.

(37) Domingo, C.; Loste, E.; Fraile, J. Grafting of Trialkoxysilane on the Surface of Nanoparticles by Conventional Wet Alcoholic and Supercritical Carbon Dioxide Deposition Methods. *J. Supercrit. Fluids* **2006**, *37* (1), 72–86.

(38) Lopez-Periago, A. M.; Sandoval, W.; Domingo, C. Chemical Modification of Nanometric

TiO2 Particles by Anchoring Functional Silane Molecules in Supercritical CO2. *Appl. Surf. Sci.* **2014**, *296*, 114–123.

(39) Purcar, V.; Cinteza, O.; Donescu, D.; Bala, D.; Ghiurea, M.; Petcu, C.; Caprarescu, S. Surface Modification of Silica Particles Assisted by CO2. *J. Supercrit. Fluids* **2014**, *87*, 34–39.

(40) Sanz-Moral, L. M.; Rueda, M.; Nieto, A.; Novak, Z.; Knez, Ž.; Martín, Á. Gradual Hydrophobic Surface Functionalization of Dry Silica Aerogels by Reaction with Silane Precursors Dissolved in Supercritical Carbon Dioxide. *J. Supercrit. Fluids* **2013**, *84*, 74–79.

(41) García-Gonzaĺez, C. A.; Fraile, J.; Lopẻz-Periago, A.; Saurina, J.; Domingo, C. Measurements and Correlation of Octyltriethoxysilane Solubility in Supercritical CO2 and Assembly of Functional Silane Monolayers on the Surface of Nanometric Particles. *Ind. Eng. Chem. Res.* **2009**, *48* (22), 9952–9960.

(42) Kendall, J. L.; Canelas, D. a.; Young, J. L.; DeSimone, J. M. Polymerizations in Supercritical Carbon Dioxide. *Chem. Rev.* **1999**, *99* (2), 543–564.

(43) Li, D.; Han, B.; Liu, Z. Grafting of 2-Hydroxyethyl Methacrylate onto Isotactic Poly (Propylene) Using Supercritical CO 2 as a Solvent and Swelling Agent. **2001**, 2187–2194.

(44) Sanli, D.; Erkey, C. Silylation from Supercritical Carbon Dioxide : A Powerful Technique for Modification of Surfaces. *J. Mater. Sci.* **2015**, *50* (22), 7159–7181.

(45) Loi, S.; Sun, G.; Franz, V.; Butt, H. J. Rupture of Molecular Thin Films Observed in Atomic Force Microscopy. II. Experiment. *Phys. Rev. E - Stat. Physics, Plasmas, Fluids, Relat. Interdiscip. Top.* **2002**, *66* (3), 1–7.

(46) Butt, H. J.; Franz, V. Rupture of Molecular Thin Films Observed in Atomic Force Microscopy. I. Theory. *Phys. Rev. E - Stat. Physics, Plasmas, Fluids, Relat. Interdiscip. Top.* **2002**, *66* (3), 1–9.

(47) Sababi, M.; Kettle, J.; Rautkoski, H.; Claesson, P. M.; Thormann, E. Structural and Nanomechanical Properties of Paperboard Coatings Studied by Peak Force Tapping Atomic Force Microscopy.

(48) Calzado-Martín, A.; Encinar, M.; Tamayo, J.; Calleja, M.; San Paulo, A. Effect of Actin Organization on the Stiffness of Living Breast Cancer Cells Revealed by Peak- Force Modulation Atomic Force Microscopy.

(49) Matsura, V.; Guari, Y.; Larionova, J.; Guérin, C.; Caneschi, A.; Sangregorio, C.; Lancelle-Beltran, E.; Mehdi, A.; Corriu, R. J. P. Synthesis of Magnetic Silica-Based Nanocomposites Containing Fe3O4 Nanoparticles. *J. Mater. Chem.* **2004**, *14*, 3026–3033.

(50) Shirley, D. A. High-Resolution X-Ray Photoemission Spectrum of the Valence Bands of Gold. *Phys. Rev. B* **1972**, *5* (12), 4709–4714.

(51) O'Hare, L.-A.; Parbhoo, B.; Leadley, S. R. Development of a Methodology for XPS Curve-Fitting of the Si 2p Core Level of Siloxane Materials. *Surf. Interface Anal.* **2004**, *36*, 1427–1434.

(52) Weeks, B. L.; Vaughn, M. W.; Deyoreo, J. J. Direct Imaging of Meniscus Formation in Atomic Force Microscopy Using Environmental Scanning Electron Microscopy. *Langmuir* **2005**, *21*, 8096–8098.

(53) Heinz, W. F.; Hoh, J. H. Spatially Resolved Force Spectroscopy of Biological Surfaces

Using the Atomic Force Microscopy. *Nanotechnology* **1999**, *17*, 143–150.

(54) Horr, T. J.; Arora, P. S. Determination of the Acid-Base Properties for 3-Amino, 3-Chloro and 3- Mercaptopropyltrimethoxysilane Coatings on Silica Surfaces by Xps. *Colloids Surfaces A Physicochem. Eng. Asp.* **1997**, *126* (2–3), 113–121.

(55) Aswal, V. K.; Goyal, P. S. Mixed Micelles of Alkyltrimethylammonium Halides A Small-Angle Neutron-Scattering Study. *Pysica B* **1998**, *245*, 73–80.

(56) Baum, M.; Rébiscoul, D.; Tardif, S.; Tas, N.; Mercury, L.; Rieutord, F. X-Ray Reflectivity Analysis of SiO2 Nanochannels Filled with Water and Ions: A New Method for the Determination of the Spatial Distribution of Ions inside Confined Media. *Procedia Earth Planet. Sci.* **2017**, *17*, 682–685.

For Table of Contents Only